Progress In Electromagnetics Research C, Vol. 132, 51–63, 2023

A High Gain CPW Fed Metamaterial Antenna for UWB Applications

Deepa Negi[1, *] and Rajesh Khanna[2]

Abstract—A multi-resonating coplanar waveguide (CPW) fed flexible antenna using metamaterial unit cell is designed for various UWB wireless communication systems. The designed unit cell has the total dimension of 14.8 mm × 14.8 mm × 0.25 mm. The top layer of the cell has a circular ring slot combined with four modified T shaped radiators giving metamaterial characteristics. The unit cell uses perfect boundary conditions along with y axis wave propagation, and it gives wide NRI region covering 2 to 16 GHz of frequency range. The overall gain of proposed CPW fed antenna is increased by using a 3×3 metamaterial array as reflector at the back of antenna. The metamaterial antenna has 2 to 16 GHz of total bandwidth and peak gain of 13.1 dB. Further the measured outcomes are in accordance with the simulated ones.

1. INTRODUCTION

Metamaterials are unique structures developed to show features and properties which are not achieved by naturally occurring substances. The features of these materials are dependent on their geometry rather than the material used for designing. Veselago [1] in 1968 found left-handed metamaterial (LHM) which shows simultaneous negative values for ε and μ and experimentally validated by Smith et al. [2]. Negative permittivity can be observed in some natural substances, however it is quite rare to find negative permeability. Further it is hard to achieve negative refractive index (NRI) and double negative (DNG) features. Different uses of metamaterial are solar cells [3], antenna structure [4, 5], super lens [6, 7], reduction in SAR [8, 9], invisibility cloaking [10, 11], filter designs [12–14], band stop structures and absorbers.

Among the various designs utilized for DNG features, the alphabet shaped designs [15–18] with a few latest structures [19–21] are more favored. Further the metamaterials are mostly used in two ways to strengthen the various antenna properties. The first is to load it as unit cell [22–30], and the second is to utilize it as reflective layer [31–35]. The common issue encountered by most wideband antenna engineers is to achieve optimal antenna size, bandwidth, radiation, and gain features. Amongst different methods, the utilization of metamaterial cells to improve antenna performance is used extensively these days. The metamaterial cells are loaded on wideband antennas from [22–30], and further 6.9 dBi of high gain is obtained in both [23, 30] along with lower bandwidth values (below 4.5 GHz). The 10.4 GHz of bandwidth value along with only 4 dBi gain is achieved in [22]. The disparity between bandwidth and gain improvement is quite visible in the above paper despite their compact dimension. The metamaterial cells are used as reflective layer or metasurfaces along with wideband antennas from [31–35], Reference [34] gives 11.9 dBi of high gain with 0.7 GHz of low bandwidth. In [35], 2.5 GHz of high bandwidth is obtained; however, gain values are not reported. In addition, these designs have huge dimensions along with multi-layered structures. These structures also display a similar disparity in the

Received 23 December 2022, Accepted 29 March 2023, Scheduled 12 April 2023
* Corresponding author: Deepa Negi (deepa.negi@chitkara.edu.in).
[1] Chitkara University Institute of Engineering and Technology, Chitkara University, Punjab, India. [2] Department of Electronics and Communication Engineering, Thapar Institute of Engineering and Technology, Patiala, India.

bandwidth and gain values as observed above. It is found that both (to load on antenna and to use a reflector layer) utilizations of metamaterials either to place on antenna design or to utilize as reflective layer, completely rely on designer's needs as well as application point of view. Here we designed an ultra-wideband (UWB) metamaterial antenna having wideband gain improvement in addition to optimal dimensions, bandwidth, and improved radiation features.

The remaining paper is arranged as follows. Section 2 discusses the design of proposed multi-resonating elliptical shape modified antenna with the impedance bandwidth of 3 to 16 GHz and peak gain of 5.8 dB, and its complete structural evolution and obtained results are also shown. Section 3 presents single sided resonator based DNG (4.8 to 6 GHz) unit cell structure with its electric and magnetic field distributions. Section 4 discusses the final unified antenna containing 3×3 array of unit cells at 14 mm of air gap from the initial antenna with impedance bandwidth 2 to 16 GHz and 13.1 dB peak gain. The improvement in elliptical modified antenna gain, bandwidth, and radiation properties is clearly observed. Section 5 shows the comparison of designed metamaterial antenna with previous structures, and at last Section 6 contains a short conclusion of work presented.

2. WIDEBAND ANTENNA STRUCTURE

The final structure of designed wideband antenna that is experimentally tested and manufactured using FR4 having 4.4 of relative permittivity and 0.25 mm of thickness is displayed in Fig. 1(a) and Fig. 1(b). The optimized measurements of proposed structure are also displayed in Table 1. The primary design of proposed structure includes an ellipse-shaped patch along with 50 Ω coplanar waveguide (CPW) feeding technique. The main motive for using this specific type of design is that elliptical patch antennas mostly provide higher operating bandwidth [36, 37], and CPW feed provides larger bandwidth as well as good unification with different circuital modules [38, 39]. Moreover, to acquire wideband characteristics in the proposed antenna, a modified slot is inserted in the middle of the ellipse-shaped radiating patch. The step by step structural progression of designed wideband structure is shown in Fig. 2; however, the effect on the corresponding reflection coefficient and gain plots of the proposed antenna are shown in Fig. 3(a) and Fig. 3(b).

Table 1. Optimized measurements of designed wideband antenna.

Parameters	Dimensions (mm)	Parameters	Dimensions (mm)
a	40	e	3.44
b	50	f	17.9
c	11.67	g	29.65
d	0.43	h	27.77

At initial stage (S1), an ellipse shaped radiating patch having CPW feed (Fig. 2) generates a multi-resonating reflection coefficient curve covering 3.8 to 16 GHz due to the overlapping of various resonance frequencies as shown in Fig. 3(a). At the next phase (S2), alterations in radiating patch lead to the bandwidth enhancement at lower frequency range resulting in the 2 GHz enhancement in gain from 3.8 to 16 GHz with improved reflection coefficient values. At the final phase (S3), further modifications in the center slot cause the increment in antenna bandwidth at lower frequency end resulting in the operating bandwidth from 3 to 16 GHz along with reflection coefficient values below −20 dB at various resonance frequencies of 3.8, 5.8, 8.8, 11.1, 13, and 16 GHz. The designed wideband antenna is fabricated, and corresponding reflection coefficient curve is experimentally measured using the KEYSIGHT E5063A (100 KHz–18 GHz) vector network analyzer. The measured gain of proposed design is shown in Fig. 3(a). It is seen that the antenna gain is improved at each stage resulting in the consistent gain values above 2.5 dB across the entire working frequency range from 2 to 16 GHz with the maximum gain value of 5.8 dB and minimum gain value of 2.8 dB in the final stage.

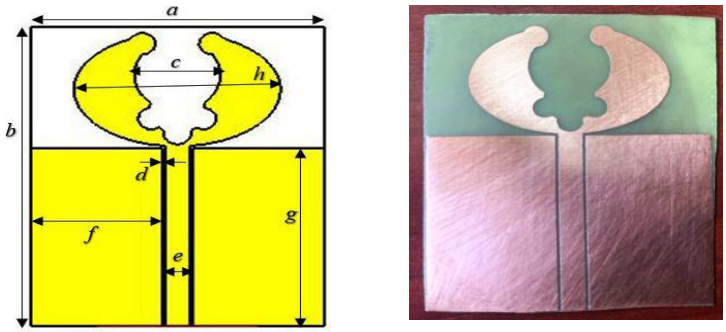

(a) (b)

Figure 1. Final structure of designed wideband antenna. (a) Simulated. (b) Fabricated.

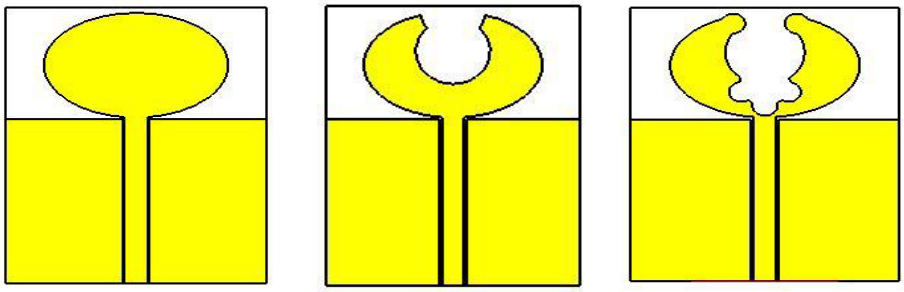

Basic antenna (S1) Antenna with modified patch (S2) Final antenna (S3)

Figure 2. Structural progression of designed wideband antenna.

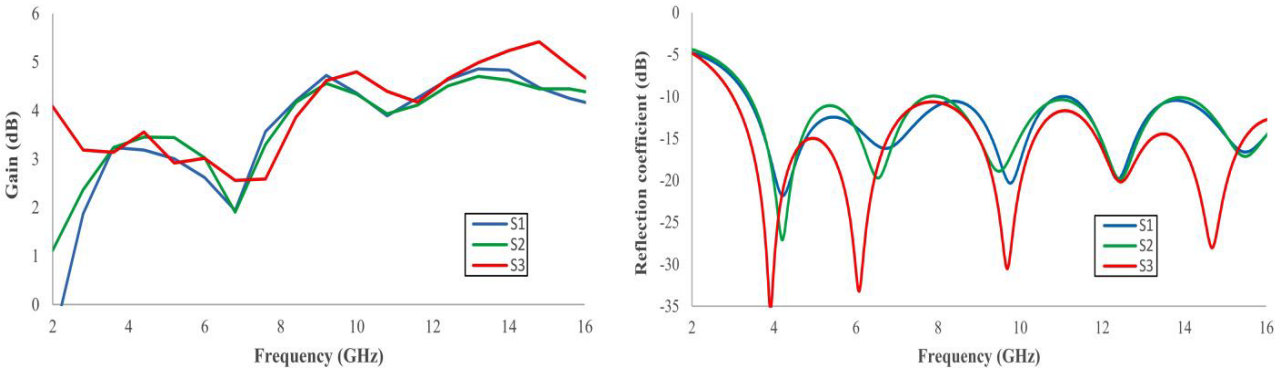

(a) (b)

Figure 3. Effect of antenna structural evolution on (a) realized gain, (b) reflection coefficient.

3. OPTIMIZED STRUCTURE OF UNIT CELL

The final DNG single sided metamaterial showing stopband characteristics is shown in Fig. 4(a). The corresponding optimized structural specifications of proposed cell are given in Table 2. For simulating a metamaterial cell, perfect magnetic and electric boundaries are utilized in both the z and x axes along with open boundaries in the y axis. The metamaterial is placed in the middle of waveguide ports along y-axis with perfect boundary conditions at remaining axis suggesting the propagation of

Table 2. Optimized measurements of designed metamaterial.

Parameters	Dimensions (mm)	Parameters	Dimensions (mm)
L_1	14.8	g_3	0.6
W_1	14.8	h_1	2.5
g_1	2.15	h_2	4.78
g_2	2.13	h_3	1.6

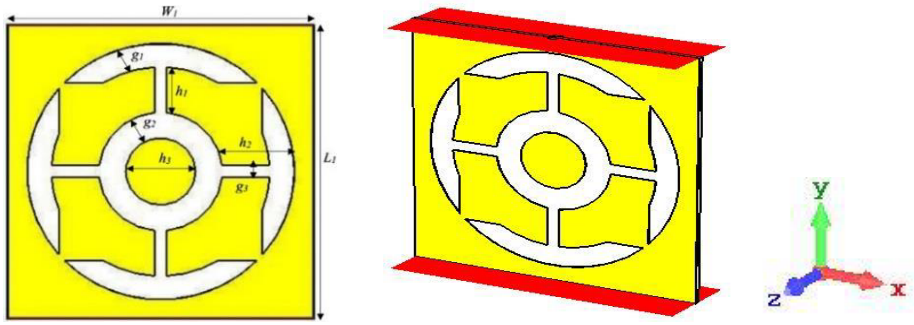

(a) (b)

Figure 4. Structure of improved metamaterial. (a) Front view. (b) Simulation prototype along with perfect boundaries.

electromagnetic waves through y-axis. The simulating design prototype along with perfect boundaries is displayed in Fig. 4(b). An FR4 substrate with 4.4 of relative permittivity and 0.25 mm of height is utilized for manufacturing and designing of the proposed metamaterial since it is cheap, conformal, and well accessible in the marketplace. All the copper components of designed unit cell have the thickness of 0.035 mm.

It is analyzed from the scattering parameter (S_{21}) of the designed metamaterial (Fig. 5(a)) that it shows the total stopband characteristics rather than the passband characteristics. By analyzing the S_{21} curve, it is found that the designed metamaterial behaves as a broadband band gap structure having 13.6 GHz of a huge stopband region in the RF bands of S, C, X, and Ku. It displays stopband characteristics in 2 to 4.8 GHz (2.8 GHz) and 5.2 to 16 GHz (10.8 GHz) of frequency regions. Additionally, in the corresponding phase plot of S_{21} parameter as described in Fig. 5(b), at various resonant frequencies, the 0° reflection in phase plots can be seen. Now to demonstrate the resonance nature and to recognize the physical characteristics of proposed metamaterial, the electric and magnetic field concentrations are studied at various resonance frequencies of 3 GHz, 5 GHz, and 10 GHz, which are selected from the band-stop areas of S_{21} plot.

3.1. Characterization of Unit Cell

The complete characterization of designed metamaterial is partitioned into two distinct steps. At first step, the proposed metamaterial is simulated to derive the scattering parameter as analyzed in the above section (Fig. 5(a)). At next step, various material characteristics of proposed unit cell including effective permittivity (ε), effective permeability (μ), wave impedance (z_m), and index of refraction (n) are derived from the acquired scattering parameters utilizing Equations (1), (2), (3), and (4), which are based upon the scattering parameter retrieval technique [40, 41].

$$z_m = \sqrt{\frac{(1+S_{11})^2 - {S_{21}}^2}{(1-S_{11})^2 - {S_{21}}^2}} \tag{1}$$

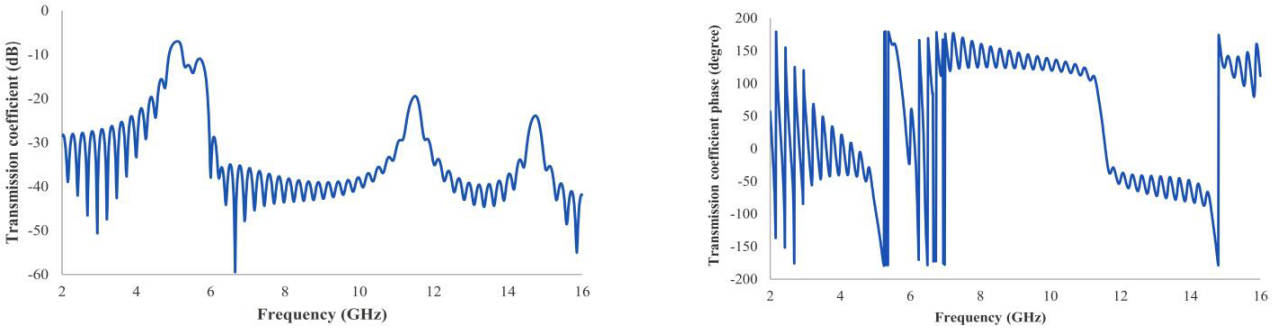

Figure 5. Scattering parameters of proposed unit cell. (a) Magnitude plot. (b) Phase plot.

$$n = \frac{1}{kq}\cos^{-1}\left[\frac{1}{2S_{21}}\left(1 - S_{11}^2 + S_{21}^2\right)\right] \tag{2}$$

$$\varepsilon = \frac{n}{z_m} \tag{3}$$

$$\mu = nz_m \tag{4}$$

here $\varepsilon, n, \mu, k, q$, and z_m denote the permittivity, index of refraction, permeability, wave vector, substrate height, and wave impedance of the metamaterial. Fig. 6 displays effective parameters (permeability, permittivity along with index of refraction) against frequency curves of the designed metamaterial.

The real components of permittivity curve as seen in Fig. 6(a) display negative values in frequency

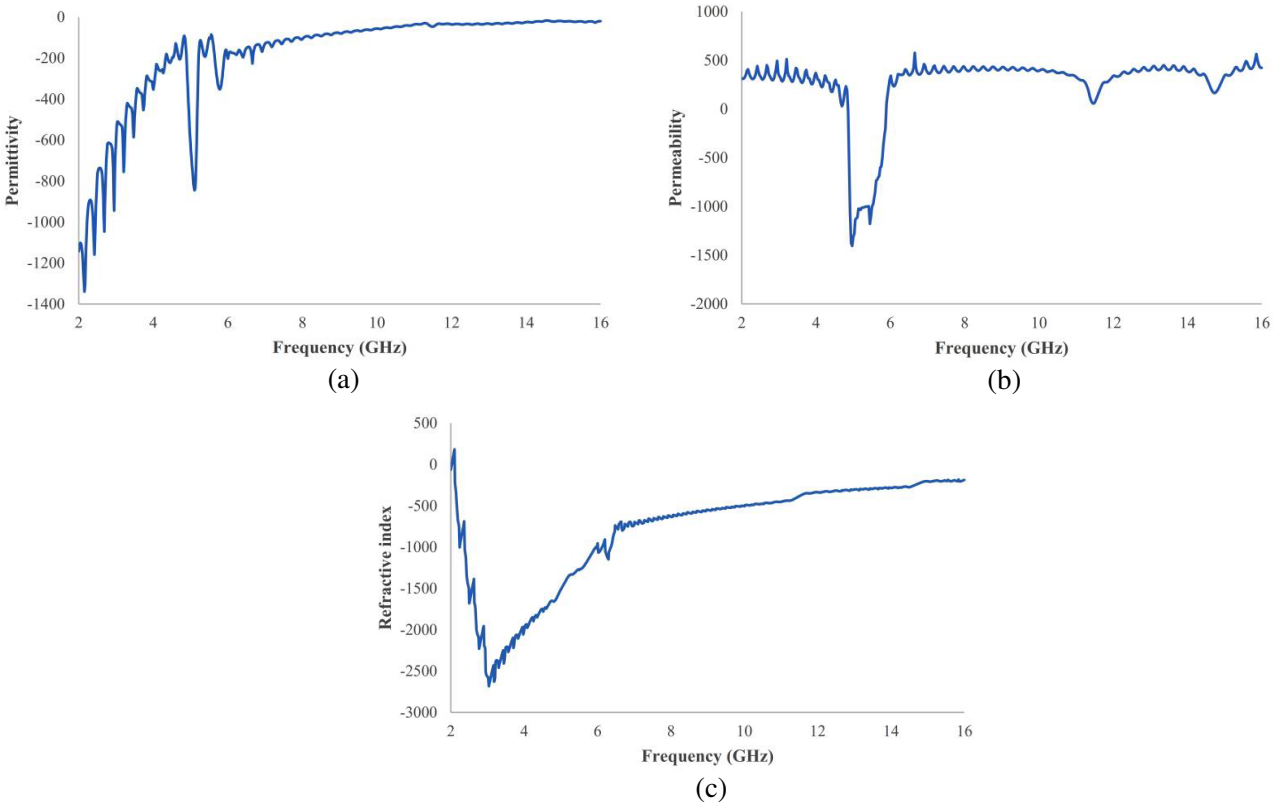

Figure 6. Retrieved characteristics of designed metamaterial showing (a) electric permittivity, (b) magnetic permeability, (c) index of refraction.

region from 2 GHz to 16 GHz, hence enveloping the RF bands like S, C, X, and Ku. The negative permeability values are observed in the frequency regions covering 4.8 to 6 GHz (1.2 GHz) enveloping C microwave band as seen in Fig. 6(b). From Fig. 6(c) the negative n values can be seen in the frequency regions covering 2 to 16 GHz along with S, C, X, and Ku microwave bands. Table 3 displays effective variables of designed metamaterial together with values of S_{21} at the resonance frequencies of 4.8 and 5.8 GHz. The specific frequency areas showing negative μ and ε values at the same time called DNG regions are found in Table 3. It is found that negative n values are observed in various other frequency regions as well apart from the DNG areas only. The n negative region, generated because of single negative characteristics, is found mainly because of the interactions between the imaginary and real components of the permeability and permittivity values. Further the proposed metamaterials display negative values of ε, μ and n in distinct frequency bands, hence it is quite noticeable that the designed DNG metamaterial shows negative values at 4.8 GHz and 5.8 GHz for all the effective variables that are displayed in Table 3.

Table 3. Real components of three effective variables (ε, μ and n) together with S_{21} values.

Effective parameters	Frequency range (GHz)	Covered bands	Values at 4.8 and 5.8 GHz
Transmission coefficient (S_{21})	2–4.8 and 5.2–16 (13.6 GHz)	S, C, X, Ku	−15 dB, −15 dB
Effective permittivity (ε)	2–16 (14 GHz)	S, C, X, Ku	−192, −332
Effective permeability (μ)	4.8–6 (1.2 GHz)	C	−132, −205
Refractive index (n)	2–16 (14 GHz)	S, C, X, Ku	−1626, −1100

3.2. Electric and Magnetic Field Concentration at Various Resonance Frequencies

Figure 7 displays the magnetic field concentration of designed antenna at three resonance frequencies. At resonance frequency of 3 GHz the magnetic field distribution at top and bottom areas of outer concentric ring structure is larger than remaining cell size. The density of magnetic field is found to be the largest at 5 GHz of resonance frequency and is mostly produced by top and bottom regions of outer concentric ring. Further at 10 GHz frequency, low intensity magnetic field density is seen only in a few specific areas. The field concentration is found to be the largest at 5 GHz and smallest at 10 GHz. Hence, it can be concluded that the total magnetic field concentration is achieved mostly because of the self and mutual inductance of various resonating structures of the unit cell.

Electric field concentration at different resonating frequencies including 3, 5, and 10 GHz is displayed in Fig. 8. In this figure, the distribution of electric field is found to be largest at 5 GHz and is highly intensive in the boundary of center ring structure along with the four connecting metallic strips. However, the higher field distribution at 3 GHz can be seen in a few specific regions including lower part of middle ring and connecting strips. The smallest field distribution is observed at 10 GHz. Here the largest field distribution is seen at 5 GHz while the smallest density is seen at 10 GHz as seen in Fig. 8(b) and Fig. 8(c).

By scrutinizing the analyses done above, it can be concluded that the stopbands generated at 3 GHz and 10 GHz are mainly because of electric resonant nature, and the stopband at 5 GHz is produced because of electric as well as magnetic resonant nature of the metamaterial. The resonance nature found at various frequencies is also validated in Fig. 6, in which negative ε having −521.5 and −56 values is seen at 3 GHz and 10 GHz frequency along with simultaneous negative ε and μ of −776.1 and −1306.9 values found at 5 GHz of resonance frequency.

4. UNIFIED ANTENNA STRUCTURE

The final unified antenna is proposed by combining the wideband antenna with an array of DNG metamaterial. The 3×3 array of proposed metamaterial cells is chosen as the optimum array size to achieve maximum outputs as shown in Fig. 9(a), as it decently shields the entire area of designed

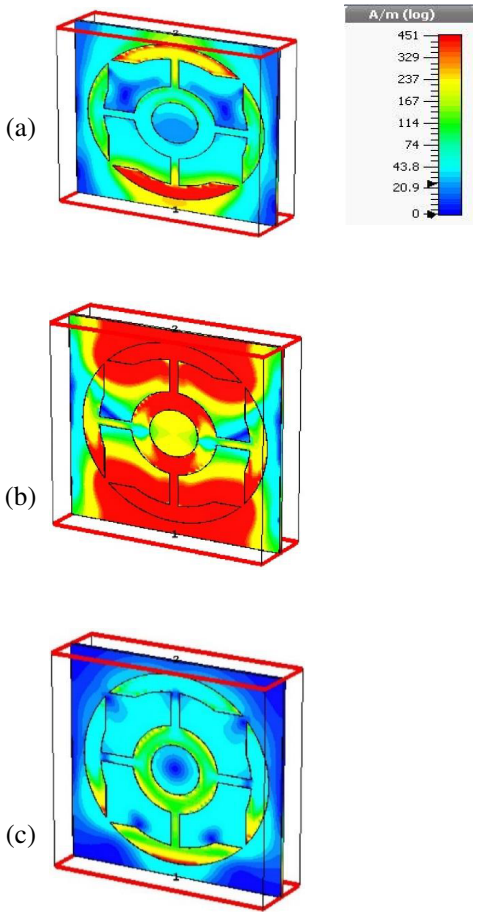

Figure 7. Magnetic field distribution at various resonance frequencies of (a) 3 GHz, (b) 5 GHz, (c) 10 GHz.

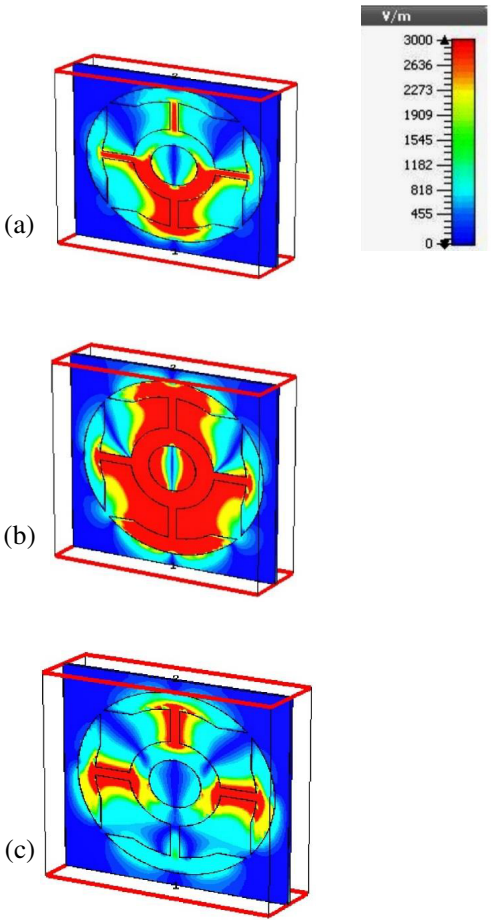

Figure 8. Electric field distribution at various resonance frequencies of (a) 3 GHz, (b) 5 GHz, (c) 10 GHz.

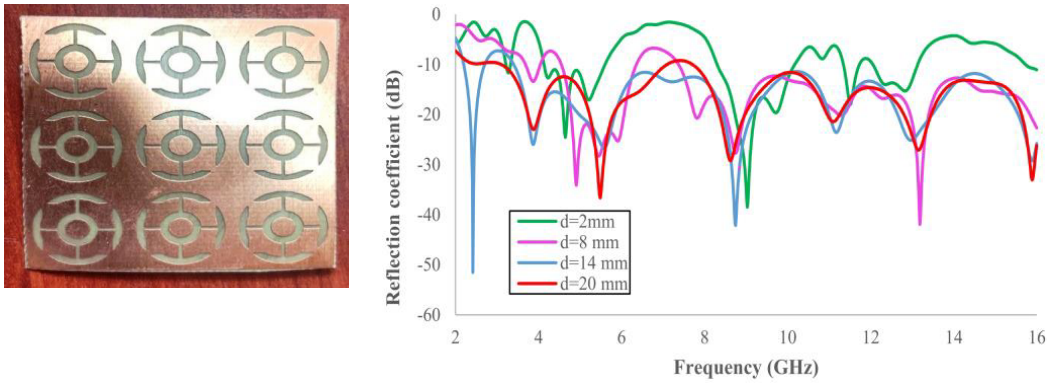

Figure 9. (a) 3×3 metamaterial layer. (b) Impact of modifying air space "d" value on reflection coefficient curve of unified structure.

wideband antenna, and further the complete antenna volume requires to be compact in size so that it can be suitable for wearable utilizations as well. The fabrication technique used is the screen-printing followed by a chemical itching process. To measure the metamaterial layer, the free space measurement

technique is used [42]. To achieve the best performance from the designed unified antenna, the metamaterial layer cannot be positioned directly over the antenna structure without any intermediate space. Therefore, a fixed air space "d" or gap needs to be established in between the metamaterial layer and antenna structure, and in practical scenarios a foam substrate is utilized to obtain the desired air separation. The impact of alterations in the value of air space "d" ranging from 2 mm to 20 mm on the unified antenna's (antenna along with metamaterial layer) S_{11} curve is displayed in Fig. 9(b). It is found that at closer air space value, the unified antenna is not able to cover the complete UWB frequency range. With increasing "d" value, the overall antenna bandwidth is also increased, and further at air space value of 14 mm, the unified antenna covers the complete UWB region from 2.1 to 16 GHz. As we increase the air space above 14 mm, the acquired operating bandwidth remains unaffected. Hence, it is observed that increasing the air space value above 14 mm simply results in the increment in overall dimension of the unified antenna. It is also found that keeping the metamaterial layer in close proximity to wideband antenna develops impedance mismatch conditions; however as we place metamaterial layer at a greater distance from the unified antenna, better matching conditions are achieved. At last, it is concluded that the best possible outcomes are achieved by using a 3×3 element metamaterial layer along with air separation value of 14 mm. The final manufactured unified antenna with the air separation of 14 mm is displayed in Fig. 10(a).

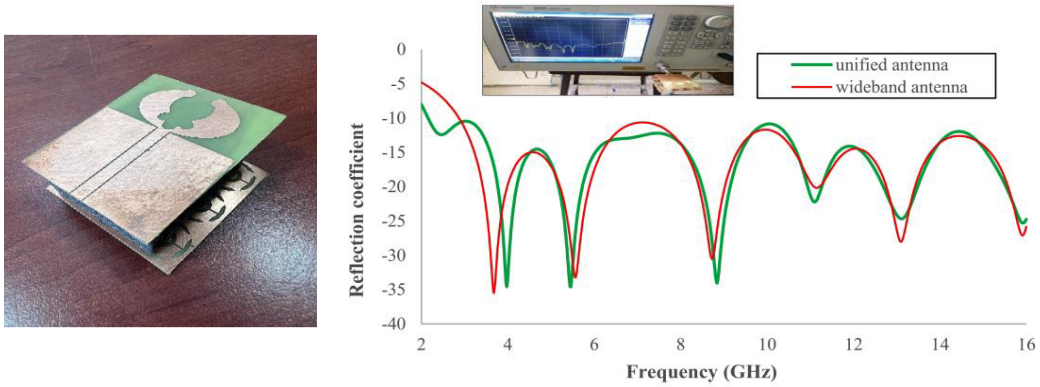

(a) (b)

Figure 10. (a) Manufactured unified antenna along with air gap of 14 mm. (b) Measured reflection coefficient curve of wideband and unified antenna.

Measured reflection coefficient plots of unified antenna along with wideband antenna are displayed in Fig. 10(b). The unified antenna is observed to envelope the wide frequency ranges from 2 to 16 GHz along with satisfactory matching conditions (under -20 dB) amongst its various resonance frequencies of 2.4, 3.9, 5.5, 8.7, 11.1, 12.9, and 15.8 GHz. Moreover, bandwidth plot is observed to enhance in the lower frequency region together with slight shift in the reflection coefficient values in the complete working frequency range as compared to the initial wideband antenna. The measured gain plots for both the wideband and unified structure are shown in Fig. 11. Gain values acquired at various resonance frequencies for the wideband antenna and unified antenna are displayed in Table 4. It is found that the metamaterial layer enhanced the gain values obtained at various resonance frequencies. At 2.4, 8.7, 12.9, and 15.8 GHz of frequencies, above 2 dB gain enhancement is found; however at 3.9, 5.5, and 11.1 GHz of resonance frequency, more than 1 dB gain enhancement is observed.

The measured radiation characteristics of both the wideband antenna along with unified antenna at various resonance frequencies of 2.4, 8.7, and 15.8 GHz are displayed in Fig. 12. It is found that the forward radiation features of unified antenna have been enhanced together with reduction in the magnitude of back and side lobes. Moreover at bigger resonance frequencies, numerous side lobes and peaks are also found, due to the radiations because of higher level of modes. It is found that in E plane pattern of unified antenna the magnitude of main lobe is enhanced from 3.17 to 8.1 dBi, 2.3 to 5.45 dBi, and 1.82 to 6.8 dBi at 2.4, 8.7 and 15.8 GHz of resonance frequencies. In the H plane pattern of unified structure, the magnitude of main lobe is enhanced from 4.6 to 8.4 dBi, 2.7 to 6.1 dBi, and 3.1 to 8.1 dBi at 2.4, 8.7, and 15.8 GHz.

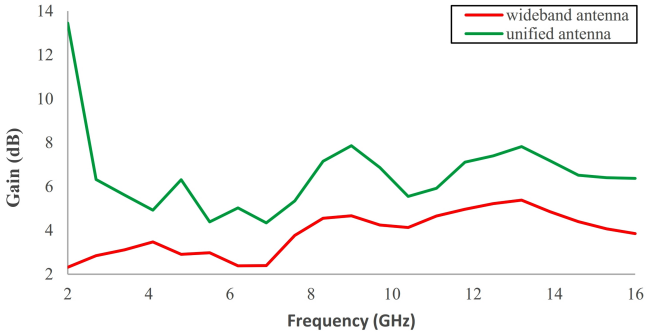

Figure 11. Gain curve of designed wideband and unified antenna.

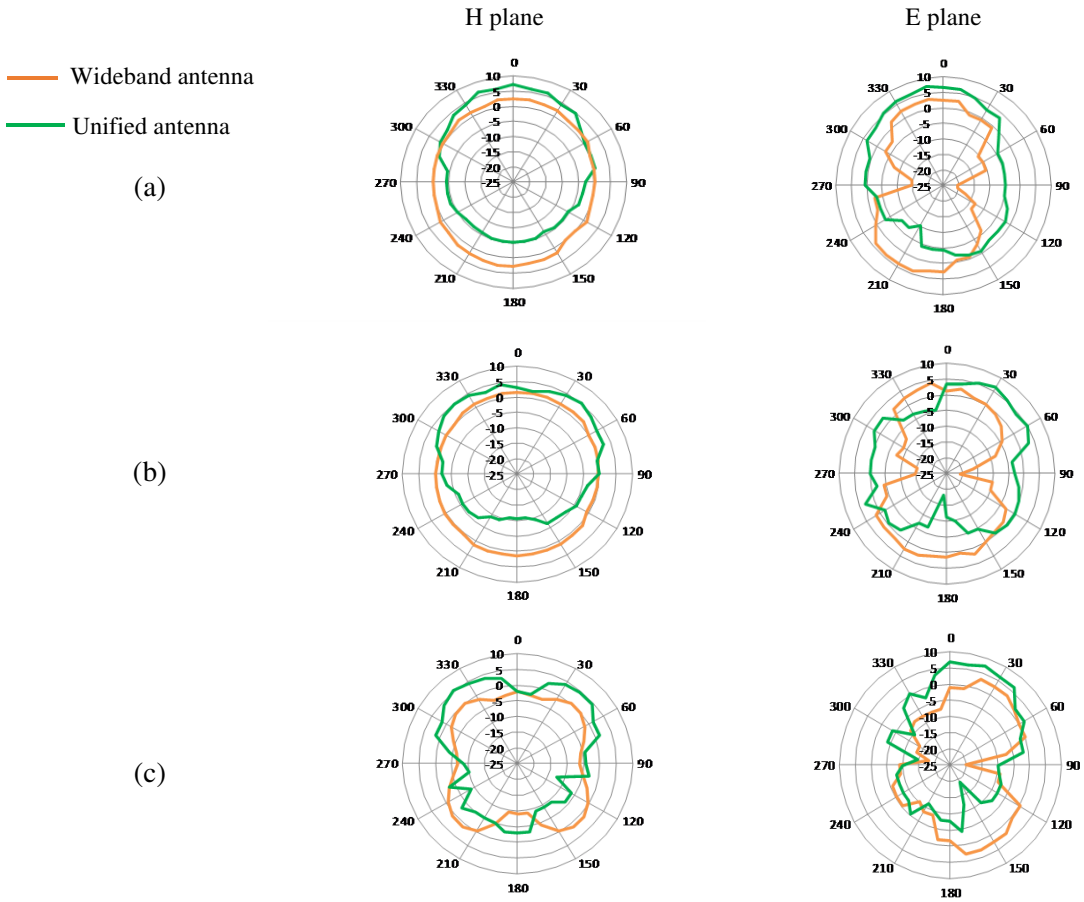

Figure 12. Measured radiation characteristics of designed wideband and unified structure (a) 2.4 GHz, (b) 8.7 GHz, (c) 15.8 GHz.

5. COMPARISON WITH PREVIOUS STRUCTURES

Here unified antenna is differentiated with earlier designed structures as displayed in Table 5. It is found that the proposed antenna has higher gain of 13.1 dB and attains 14 GHz of maximum bandwidth along with conformal structure than previous papers. The metamaterial structures utilized in many articles are mostly motivated by earlier reported designs like spiral designs, split ring resonators (SRRs), and altered alphabetical structures excluding [32, 33, 42–44] and present work, where novel metamaterial

designs are utilized. Moreover, in [22, 24–26, 28–30] unit cells are loaded on antenna because of which they have smaller dimensions along with fewer cells than [31–37] where metamaterial array is used as the reflective layer. Compared to other papers [31–37] where metamaterials are used as a layer the present antenna has smaller volume except [31, 32]; however, the proposed antennas gain and bandwidth values are much better. The bandwidth and gain tradeoff can be found clearly in all the articles analyzed in Table 5. The proposed design displays optimum bandwidth as well as gain values. It is visible that the designed metamaterial antenna has better outcomes and distinctly surpasses the previously reported metamaterial antennas.

Table 4. Obtained gain values for both the wideband and unified antenna.

Frequencies (GHz)	Gain values for wideband antenna (dB)	Gain values for unified antenna (dB)
2.4	2.6	9.2
3.9	3.3	5.1
5.5	2.9	4.4
8.7	4.6	7.6
11.1	4.6	5.9
12.9	5.3	7.6
15.8	3.8	6.3

Table 5. Comparison of designed structure with earlier reported structures.

Ref.	Cell dimension/ Total volume (mm^3)	Impedance bandwidth (GHz)	Cells utilized	Total size/volume (mm^3)	Highest gain (dB)	Flexible /Non-Flexible (F/NF)	Cell design
22	NA	3.1–13.5 (10.4)	3	25 × 22 × 1.6 (880)	4	NF	Split ring resonators (SRRs)
24	NA	3.9–13.2 (9.3)	2	25 × 15 × 1.6 (600)	4.8	NF	Concentric structure
25	NA	2.5–2.78, 3.24–4, 5.18–5.88 (1.74)	1	35 × 35 × 1 (1225)	3.94	NF	Electric-inductive-capacitive (ELC) resonator
26	7 × 7 × 1.6/78.4	3.1–10.71 (7.61)	(2 × 4) array	26 × 12 × 1.6 (499.2)	3.9	NF	SRRs
28	NA	4–12.5 (8.5)	4	25 × 15 × 1.6 (600)	4.5	NF	Spiral structure
29	NA	24–30 (6)	1	5 × 6 × 0.8 (24)	3	NF	Complimentary SRRs
30	NA	3.5–7.9 (4.4)	12	32 × 28 × 0.794 (711.4)	6.9	NF	Planar structure
31	NA	4.45–5.71 (1.26)	(4 × 4) array	44 × 35 × 4 (6160)	6.6	NF	Spiral structure

32	5.3 × 5.3 × 0.5/14.045	9.65–10.1 (0.45)	(3 × 3) array	89 × 50 × 4.075 (18133.7)	8.24	NF	Novel structure
33	18 × 20 × 3.048/1097.28	5.47–7.25 (1.78)	(2 × 2) on top and (2 × 5) on the bottom	137 × 77 × 3.048 (32153.3)	9.2	NF	Novel structure
34	NA	5.4–6.1 (0.7)	2	52.5 × 67.1 × 10.96 (38609.34)	11.9	NF	SRRs
35	6 × 6 × 1.58/56.88	7.5–10 (2.5)	(9 × 13) array	NA	NA	NF	Modified alphabetical structure
43	14.8 × 14.8 × 0.15/32.9	2.3–16 (13.7)	(3 × 3) array	50 × 44.4 × 14 (31,080)	8	F	Novel structure
44	14.8 × 14.8 × 0.25/54.76	2–16 (14)	(4 × 4) array	59.2 × 59.2 × 12 (42055.6)	10.2	F	Novel structure
Proposed work	14.8 × 14.8 × 0.25/54.76	2–16 (14)	(3 × 3) array	50 × 44.4 × 12 (26,640)	13.1	F	Novel structure

6. CONCLUSIONS

In this article, a resonator-based 3×3 metamaterial array at the optimum air space of 14 mm is used as a reflector plane below a wideband antenna to obtain optimal bandwidth and gain features. Both the structures are flexible in nature with thickness 0.25 mm. With the introduction of metamaterial layer 1.8 GHz and 7.3 dB enhancement in the impedance bandwidth and gain values is observed. Complete design analysis of the proposed unit cell along with its electric and magnetic field distributions is also presented for better understanding. Metamaterial antenna displays 14 GHz of total bandwidth and maximum gain of 13.1 dB. The proposed metamaterial antenna displays better outcomes and can be viewed as a promising candidate for various present-day metamaterial-based antennas. The sole drawback of the present work is its antenna with larger dimensions. Good agreement between simulated and measured results is observed. Hence, the designed antenna can be utilized in various satellite, wearable, and wireless applications aside from UWB applications.

REFERENCES

1. Veselago, V. G., "The electrodynamics of substances with simultaneously negative values of ε and μ," *Sov. Phys.*, Vol. 10, No. 4, 509–514, 1968.
2. Smith, D. R., W. J. Padilla, D. C. Vier, S. C. Nemat-Nasser, and S. Schultz, "Composite medium with simultaneously negative permeability and permittivity," *Phys. Rev. Lett.*, Vol. 84, 4184–7, 2000.
3. Houshmand, M., M. H. Zandi, and N. E. Gorji, "Modeling of optical losses in perovskite solar cells," *Sup. Latt. Micro.*, Vol. 97, No. 1, 424–42, 2016.
4. Islam, M. M., M. T. Islam, and M. Samsuzzaman, "Faruque MRI, compact metamaterial antenna for UWB applications," *Electron. Lett.*, Vol. 51, No. 16, 1222–1224, 2015.
5. Khan, O. M., Z. U. Islam, Q. U. Islam, and F. A. Bhatti, "Multiband high- gain printed Yagi array using square spiral ring metamaterial structures for S-band applications," *IEEE Ant. Wirel. Propag. Lett.*, Vol. 13, 1100–1103, 2014.

6. Zhang, K., Y. Yuan, X. Ding, B. Ratni, S. N. Burokur, and Q. Wu, "High-efficiency metalenses with switchable functionalities in microwave region," *ACS Appl. Mater. Interfaces*, Vol. 11, No. 31, 28423–28430, 2019.
7. Li, H., G. M. Wang, T. Cai, J. G. Liang, and H. Hou, "Bifunctional circularly-polarized lenses with simultaneous geometrical and propagating phase control metasurfaces," *J. Phys. D: Appl. Phys.*, Vol. 52, No. 46, 465105, 2019,
8. Sultan, K., H. Abdullah, E. Abdallah, and E. Hashish, "Low-SAR miniaturized printed antenna for mobile, ISM, and WLAN services," *IEEE Ant. Wirel. Propag. Lett.*, Vol. 12, 1106–1109, 2013.
9. Faruque, M. R. I., M. T. Islam, and N. Misran, "Design analysis of new metamaterial for EM absorption reduction," *Progress In Electromagnetics Research*, Vol. 124, 119–135, 2012.
10. Kaur, S. and H. J. Kaur, "Comparative analysis of plasmonic metamaterial absorber for noble, alkaline earth and transition metals in visible region," *6th International Conference on Computing for Sustainable Global Development*, 513–516, 2019.
11. Hossain, K., T. Sabapathy, M. Jusoh, et al., "Electrically tunable left-handed textile metamaterial for microwave applications," *Materials*, Vol. 14, No. 5, 1274, 2021.
12. Fang, C. Y., J. S. Gao, and H. Liu, "A novel metamaterial filter with stable passband performance based on frequency selective surface," *AIP Advances*, Vol. 4, No. 7, 077114, 2014.
13. Alam, M. J., M. R. I. Faruque, and M. T. Islam, "Labyrinth double split open loop resonator-based band pass filter design for S, C and X-band application," *J. Phys. D: Appl. Phys.*, Vol. 51, No. 26, 1–8, 2018.
14. Singh, R., I. Al-Naib, W. Cao, C. Rockstuhl, M. Koch, and W. Zhang, "The Fano resonance in symmetry broken terahertz metamaterials," *IEEE Trans. Terahertz Sci. Technol.*, Vol. 3, No. 6, 1–7, 2013.
15. Zhou, Z. and H. Yang, "Triple-band asymmetric transmission of linear polarization with deformed S-shape bilayer chiral metamaterial," *Appl. Phys.*, Vol. 119, No. 1, 115–119, 2015.
16. Alam, M. J., M. R. I. Faruque, M. J. Hossain, and M. T. Islam, "Depiction and analysis of a modified H-shaped double-negative meta atom for satellite communication," *Int. J. Microw. Wirel. Technol.*, Vol. 10, No. 10, 1155–1165, 2018.
17. Huangfu, J., L. Ran, H. Chen, and K. Chen, "Experimental confirmation of negative refractive index of a metamaterial composed of Ω-like metallic patterns," *Appl. Phys. Lett.*, Vol. 84, No. 9, 1537–1539, 2004.
18. Chun, Y. C., C. Y. Ping, W. Qiong, and Z. S. Chuang, "Negative refraction of a symmetrical π-shaped metamaterial," *Phys. Lett.*, Vol. 25, No. 2, 482–484, 2008.
19. Hossain, M. J., M. R. I. Faraque, M. J. Alam, M. F. Mansor, and M. T. Islam, "A broadband negative refractive index meta-atom for quad-band and sensor applications," *Microw. Opt. Technol. Lett.*, Vol. 60, No. 12, 2899–2907, 2018.
20. Alam, T., F. B. Ashraf, and M. T. Islam, "Flexible paper substrate based wide band NRI metamaterial for X-band application," *Microw. Opt. Technol. Lett.*, Vol. 60, No. 5, 1309–1312, 2018.
21. Rahman, M. N., M. T. Islam, and M. Samsuzzaman, "Design and analysis of a resonator-based metamaterial for sensor applications," *Microw. Opt. Technol. Lett.*, Vol. 60, No. 3, 694–698, 2017.
22. Singh, H. S., S. Kalraiya, M. K. Meshram, and R. M. Shubair, "Metamaterial inspired CPW-fed compact antenna for ultrawide band applications," *Int. J. RF Microw. Comput. Aided. Eng.*, e21768, 2019.
23. Seshadri, A. and N. Gupta, "Modelling and analysis of metamaterial-based antenna for Wi-Fi and WLAN applications," *Adv. in Comm. Dev. Net.*, Vol. 537, 167–173, 2019.
24. Rajasekhar, N. V. and D. S. Kumar, "Metamaterial based compact UWB planar monopole antennas," *Microw. Opt. Technol. Lett.*, Vol. 60, No. 6, 1332–1338, 2018.
25. Pushkar, P. and V. R. Gupta, "A metamaterial-based tri band antenna for WiMAX/WLAN applications," *Microw. Opt. Technol. Lett.*, Vol. 58, No. 3, 558–561, 2016.

26. Mahmud, M. Z., M. T. Islam, N. Misran, M. J. Singh, and K. Mat, "A negative index metamaterial to enhance the performance of miniaturized UWB antenna for microwave imaging applications," *Appl. Sci.*, Vol. 7, 1–16, 2017.
27. Patel, S. K. and Y. Kosta, "Liquid metamaterial based microstrip antenna," *Microw. Opt. Technol. Lett.*, Vol. 60, No. 2, 318–322, 2018.
28. Nuthakki, V. R. and S. Dhamodharan, "UWB metamaterial-based miniaturized planar monopole antennas," *Int. J. Electron. Comm.*, Vol. 82, 93–103, 2017.
29. Rani, R. B. and S. K. Pandey, "Metamaterial-inspired printed UWB antenna for short range RADAR applications," *Microw. Opt. Technol. Lett.*, Vol. 59, 1597–1600, 2017.
30. Zhang, H. T., G. Q. Luo, B. Yuan, and X. H. Zhang, "A novel ultra-wideband metamaterial antenna using chessboard-shaped patch," *Microw. Opt. Technol. Lett.*, Vol. 58, No. 12, 3008–3012, 2016.
31. Arayeshnia, A., A. Bayat, M. Keshtkar-Bagheri, and S. Jarchi, "Miniaturized lowprofile antenna based on uniplanar quasi-composite right/left-handed metamaterial," *Int. J. RF Microw. Comput. Aided. Eng.*, e21888, 2019.
32. Pandit, S., A. Mohan, and P. Ray, "Metamaterial-inspired low-profile high-gain slot antenna," *Microw. Opt. Technol. Lett.*, 1–6, 2019.
33. Nguyen, N. L. and V. Y. Vu, "Gain enhancement for MIMO antenna using metamaterial structure," *Int. J. Microw. Wirel. Technol.*, 1–12, 2019.
34. Arora, C., S. S. Pattnaik, and R. N. Baral, "Metamaterial inspired DNG superstrate for performance improvement of microstrip patch antenna array," *Int. J. Microw. Wirel. Technol.*, Vol. 10, No. 3, 318–327, 2018.
35. Ghosh, J., D. Mitra, and S. R. B. Chaudhuri, "Reduction of leaky wave coupling in a superstrate loaded antenna using metamaterial," *J. Electromag. Waves. App.*, Vol. 32, No. 17, 2292–2303, 2018.
36. Sarkar, D., K. V. Srivastava, and K. Saurav, "A compact microstrip-fed triple band-notched UWB monopole antenna," *IEEE Ant. Wirel. Propag. Lett.*, Vol. 13, 396–399, 2014.
37. Sun, Y., S. W. Cheung, and T. I. Yuk, "Design of a textile ultra-wideband antenna with stable performance for body-centric wireless communications," *IET Microw. Antennas Propag.*, Vol. 8, No. 15, 1363–1375, 2014.
38. Bahrami, H., A. Mirbozorgi, R. Ameli, L. A. Rusch, and B. Gosselin, "Flexible polarization-diverse UWB antennas for implantable neural recording systems," *IEEE Trans. Biomed. Circuits Syst.*, Vol. 10, No. 1, 38–48, 2016.
39. Denidni, T. A. and M. A. Habib, "Broadband printed CPW-fed circular slot antenna," *Electron. Lett.*, Vol. 42, No. 3, 135–136, 2006.
40. Chen, X., T. M. Grzegorczyk, B. I. Wu, J. Pacheco, and J. A. Kong, "Robust method to retrieve the constitutive effective parameters of metamaterials," *Phys. Rev. E*, Vol. 70, 016608.1–016608.7, 2004.
41. Smith, D. R., D. C. Vier, T. Koschny, and C. M. Soukoulis, "Electromagnetic parameter retrieval from inhomogeneous metamaterials," *Phys. Rev. E*, Vol. 71, 036617.1–036617.11, 2005.
42. Sarkhel, A., D. Mitra, and S. R. B. Chaudhuri, "A compact metamaterial with multi-band negative-index Characteristics," *Appl. Phys. A*, Vol. 471, No. 122, 1–10, 2016.
43. Negi, D., R. Khanna, and J. Kaur, "Design and performance analysis of a conformal CPW fed wideband antenna with Mu-Negative metamaterial for wearable applications," *Int. J. Microw. Wirel. Technol.*, Vol. 11, No. 08, 1–15, 2019.
44. Negi, D., R. Khanna, and J. Kaur, "Broadband gain enhancement of an UWB antenna using conformal wideband NRI metamaterial," *Frequenz.*, Vol. 75, 3–4, 2020.